2-1-2019

Comprehensive behavioral and biochemical outcomes of novel murine models of GM1-gangliosidosis and Morquio syndrome type B

Michael J Przybilla

Li Ou

Alexandru-Flaviu Tăbăran

Xuntian Jiang

Rohini Sidhu

See next page for additional authors

Authors
Michael J Przybilla, Li Ou, Alexandru-Flaviu Tăbăran, Xuntian Jiang, Rohini Sidhu, Pamela J Kell, Daniel S Ory, M Gerard O'Sullivan, and Chester B Whitley

Molecular Genetics and Metabolism 126 (2019) 139–150

Contents lists available at ScienceDirect

Molecular Genetics and Metabolism

journal homepage: www.elsevier.com/locate/ymgme

Comprehensive behavioral and biochemical outcomes of novel murine models of GM1-gangliosidosis and Morquio syndrome type B

Michael J. Przybilla[a,b], Li Ou[a], Alexandru-Flaviu Tăbăran[c], Xuntian Jiang[d], Rohini Sidhu[d], Pamela J. Kell[d], Daniel S. Ory[d], M. Gerard O'Sullivan[c], Chester B. Whitley[a,b,*]

[a] Gene Therapy Center, Department of Pediatrics, University of Minnesota, Minneapolis, MN, United States
[b] Molecular, Cellular, Developmental Biology, and Genetics Graduate Program, University of Minnesota, Minneapolis, MN, United States
[c] Comparative Pathology Shared Resource, Masonic Cancer Center and College of Veterinary Medicine, University of Minnesota, Saint Paul, MN, United States
[d] Department of Medicine, Washington University School of Medicine, Saint Louis, MO, United States

ARTICLE INFO

Keywords:
Lysosomal disease
Gangliosidosis
Mucopolysaccharidosis
Mouse Model

ABSTRACT

Deficiencies in the lysosomal hydrolase β-galactosidase (β-gal) lead to two distinct diseases: the skeletal disease Morquio syndrome type B, and the neurodegenerative disease GM1-gangliosidosis. Utilizing CRISPR-Cas9 genome editing, the mouse β-gal encoding gene, *Glb1*, was targeted to generate both models of β-gal deficiency in a single experiment. For Morquio syndrome type B, the common human missense mutation W273L (position 274 in mice) was introduced into the *Glb1* gene ($Glb1^{W274L}$), while for GM1-gangliosidosis, a 20 bp mutation was generated to remove the catalytic nucleophile of β-gal (β-gal$^{-/-}$). $Glb1^{W274L}$ mice showed a significant reduction in β-gal enzyme activity (8.4–13.3% of wildtype), but displayed no marked phenotype after one year. In contrast, β-gal$^{-/-}$ mice were devoid of β-gal enzyme activity (≤1% of wildtype), resulting in ganglioside accumulation and severe cellular vacuolation throughout the central nervous system (CNS). β-gal$^{-/-}$ mice also displayed severe neuromotor and neurocognitive dysfunction, and as the disease progressed, the mice became emaciated and succumbed to the disease by 10 months of age. Overall, in addition to generating a novel murine model that phenotypically resembles GM1-gangliosidosis, the first model of β-galactosidase deficiency with residual enzyme activity has been developed.

1. Introduction

Typically, when a lysosomal hydrolase is defective, a single lysosomal disease arises; however, in the case of the enzyme β-galactosidase (β-gal, EC 3.2.1.23), mutations in the encoding gene, *GLB1*, can result in two lysosomal diseases: GM1-gangliosidosis (OMIM #230500, 230600, 230650), a neurodegenerative disease, and Morquio syndrome type B (Mucopolysaccharidosis IV B, MPS IVB OMIM #253010), a skeletal disease. β-gal is responsible for catabolizing the terminal galactose residue in GM1 ganglioside, its asialo derivative GA1, and the glycosaminoglycan keratan sulfate [1,2]. The primary substrates that accumulate in GM1 gangliosidosis are GM1 and GA1 gangliosides, while in Morquio syndrome type B, keratan sulfate accumulates. Clinically, GM1-gangliosidosis patients are categorized into one of three disease severities, 1) infantile, 2) late infantile/juvenile, and 3) adult, depending upon symptoms and residual β-gal enzyme activity. Those with the most severe infantile form have minimal or no residual enzyme activity. Patients usually present with symptoms around 6 months of age, including severe psychomotor and neurocognitive regression, hypotonia, macular cherry-red spot, hepatosplenomegaly, skeletal dysplasia, coarse facial features, and typically succumb to the disease by 2 years of age [3]. In Morquio syndrome type B, patients have residual β-gal enzyme activity (1.3–11.9% of normal [4–9]. Morquio syndrome type B patients present with normal intellect, but suffer from progressive skeletal dysplasia, short stature, in addition to odontoid hypoplasia and corneal clouding [10]. Besides palliative approaches, there are no available treatments for either of these debilitating diseases.

Animal models are key for the development of novel therapies for many diseases. In the case of GM1-gangliosidosis, two previously described murine models have been developed [11,12], but were not publicly available when this project was initiated; while no animal models of Morquio syndrome type B exist. The GM1-gangliosidosis mouse models that currently exist were developed utilizing embryonic stem (ES) cell gene targeting to insert the exogenous neomycin resistance gene into the *Glb1* locus. The model developed by Hahn et al. [11] disrupted the gene by inserting the cassette in exon 6, while

* Corresponding author at: Gene Therapy Center, Department of Pediatrics, 12-169 PWB, 516 Delaware St SE, Minneapolis, MN 55455, United States.
E-mail address: whitley@umn.edu (C.B. Whitley).

https://doi.org/10.1016/j.ymgme.2018.11.002
Received 4 September 2018; Received in revised form 5 November 2018; Accepted 6 November 2018
Available online 22 November 2018

Matsuda et al. [12] targeted exon 15. In both knockout models, β-gal enzyme activity is nominal compared to controls, which results in accumulation of GM1 and GA1 gangliosides. While these models have shown impaired neuromotor function [13,14], neurocognitive testing has not been conducted.

To create models of β-gal enzyme deficiency for use in the development of novel therapies, we employed CRISPR-Cas9 genome editing. Following a double-stranded DNA break, the eukaryotic cell repairs the lesion *via* two pathways: homology directed repair or non-homologous end joining [15–17]. Here we describe the exploitation of this knowledge to create two novel models of β-galactosidase deficiencies in a single experiment. To develop a model of Morquio syndrome type B, a mutation that is commonly found in patients [4–9], *GLB1*^{W273L}, was introduced into mice. Additionally, a mutation that abolished β-gal enzyme activity was created. Mice lacking β-gal activity (β-gal$^{-/-}$) recapitulated many aspects of the human disease, including ganglioside accumulation, cellular vacuolation, and a significantly shortened lifespan. Additionally, β-gal$^{-/-}$ mice had neuromotor impairment, in addition to a severe neurocognitive deficiency not previously described. Overall, β-gal$^{-/-}$ mice recapitulated many biochemical, histological, and phenotypic characteristics of human GM1-gangliosidosis. However, while mice homozygous for a common Morquio syndrome type B mutation (*Glb1*^{W274L}) had a present, but significantly reduced, β-gal enzyme activity, *Glb1*^{W274L} mice displayed no observable Morquio syndrome type B phenotype up to one year of age.

2. Materials and methods

2.1. Generation of β-gal$^{-/-}$ and Glb1^{W274L} mice by CRISPR-Cas9 embryo microinjection

β-galactosidase deficient mice were generated by Dr. Dale Cowley and the Animal Models Core Facility at the University of North Carolina at Chapel Hill utilizing CRISPR-Cas9 genome editing technology in a C57BL/6J genetic background. Candidate CRISPR-Cas9 guide RNAs (gRNA) targeting exon 8 of the mouse *Glb1* gene were designed utilizing Benchling© software (Benchling, Inc) based on the system established previously by Mali *et al.* [18]. To increase specificity and reduce the potential of off-target Cas9 cleavage, truncated 17 nucleotide gRNAs were designed, as suggested in Fu *et al.* [19]. gRNAs were produced by T7 *in vitro* transcription and validated *in vitro* by incubating a gRNA, Cas9 enzyme, and PCR amplified target site together, followed by gel electrophoresis to determine the extent of *in vitro* cleavage activity. The most efficient candidate gRNA was then used for zygote microinjection.

Zygotes for microinjection were produced by super-ovulating C57BL/6J females by injection of pregnant mare's serum gonadotropin (PMSG) and human chorionic gonadotropin (HCG) and then mated with C57BL/6J stud males. 114 one-cell embryos were collected from the ampulla oviducts the morning after mating and microinjected with 400 nM Cas9 protein, 50 ng/μl gRNA targeting exon 8 of *Glb1*, and 50 ng/μl donor oligonucleotide. For this experiment, Cas9 protein was utilized for microinjections to increase on-target efficiency of DNA cutting [20,21], but to also circumvent the issues with using Cas9 mRNA, including mosaicism at the target site [22]. The donor oligonucleotide was designed to introduce a 2 bp mutation encoding a tryptophan to leucine substitution commonly found in Morquio syndrome type B patients. Of the 114 injected zygotes, 106 were transferred into 4 pseudopregnant mothers, yielding 24 neonates (Fig. 1A). Potential founders born from microinjected embryos were screened by PCR amplification of the *Glb1* target site, followed by Sanger sequencing. Of the live offspring, two founders contained a 2 bp mutation resulting in the W274L amino acid substitution of interest, while another founder contained a 20 bp deletion. These founders were bred to C57BL/6J wildtype mice for germline transmission of the mutant alleles. N1 offspring were screened by PCR-amplification and sequencing as described for the founder animals. Heterozygous N1 animals were bred to obtain the wildtype, heterozygous, and homozygous mutant animals used in this study.

2.2. Animal care and procedures

All animal care and experimental procedures were conducted under the approval of the Institute Animal Care and Use Committee (IACUC) of the University of Minnesota. All animals were housed in specific pathogen-free conditions and genotyped by PCR. C57BL/6J (000664) animals were purchased from The Jackson Laboratory.

The humane endpoint for these studies was defined as the presence of limb paralysis, the inability to rear and feed normally, or the loss of ≥15% of peak body weight. For biochemical analysis, animals were sacrificed by CO_2 asphyxiation and perfused transcardially with 20 mL of ice-cold PBS. Animals utilized for histological analysis were further perfused with 20 mL of 10% neutral buffered formalin (NBF). Tissues isolated for biochemical assays were flash frozen in liquid nitrogen.

2.3. β-galactosidase (β-gal) enzyme assay

β-gal enzyme activity was determined utilizing a fluorometric assay as previously described [23], with slight modification. Briefly, tissue samples were homogenized in 1 mL of T-PER™ Tissue Protein Extraction Reagent (Thermo Fisher Scientific, Waltham, MA) with Halt™ Protease Inhibitor Cocktail (Thermo Fischer Scientific) added to manufacturers recommendation. To determine β-gal activity, supernatants of the tissue homogenates were diluted with a 0.2 M sodium acetate/0.1 M sodium chloride buffer (pH 4.3) and 40 μL of each was added in triplicate to a 96-well black round-bottom plate (Corning™, Corning, NY) on ice. 20 μL of a substrate solution containing 1.0 mM 4-methylumbelliferyl-β-D-galactopyranoside (4-MUGal, Millipore-Sigma, St. Louis, MO) was added to each well, and the plate was incubated for 30 min at 37 °C. To quench the reaction, 200 μL of 1 M carbonate buffer (1 M sodium carbonate to pH 10.7 with 1 M sodium bicarbonate) was added. In the presence of β-gal enzyme, the non-fluorescent 4-MUGal is cleaved and releases a fluorescent 4-methylumbelliferone (4-MU) molecule. This fluorescence was measured in a Synergy MX Plate Reader with Gen5 plate reader program (BioTek Instruments, Winooski, VT) with excitation at 360 nm and emission read at 460 nm (80% sensitivity). 4-MU (Sigma-Millipore) is used to generate a standard curve. β-gal enzyme activity is expressed in nmol of 4-MU released per hour, per milligram of protein (nmol/h/mg), which is determined using a Pierce™ BCA Protein Assay Kit (Thermo Fisher Scientific).

2.4. Histopathological analysis

Following perfusion and fixation with 10% NBF, tissues were processed into paraffin wax using standard histology techniques, sectioned at a thickness of 4 μm, stained with hematoxylin and eosin (H&E), and evaluated using light microscopy by two A.C.V.P. board-certified pathologists (A.-F. T. and M.G.O'S). Additional evaluation was performed on selected tissues stained with Luxol fast blue (LFB)/H&E combination stain, Periodic acid-Schiff (PAS), alcian blue, and toluidine blue using standard laboratory protocols. For the *Glb1*^{W274L} mice, the tissues that were examined include the lungs, liver, heart, spleen, kidney, adrenal gland, stomach, large and small intestine, brain, eyes, salivary glands, skeletal muscle, sternum, and femur (including hip and stifle joints). For β-gal$^{-/-}$ mice, major organs were examined including the brain, liver, heart, intestines, and pancreas. All work was done at the Masonic Cancer Center Comparative Pathology Shared Resource laboratory at the University of Minnesota.

2.5. Ganglioside isolation and quantification

GM1, GA1, GM2, and GM3 ganglioside accumulation in β-gal$^{-/-}$ animals was quantified by homogenizing the cerebellum (1 g wet

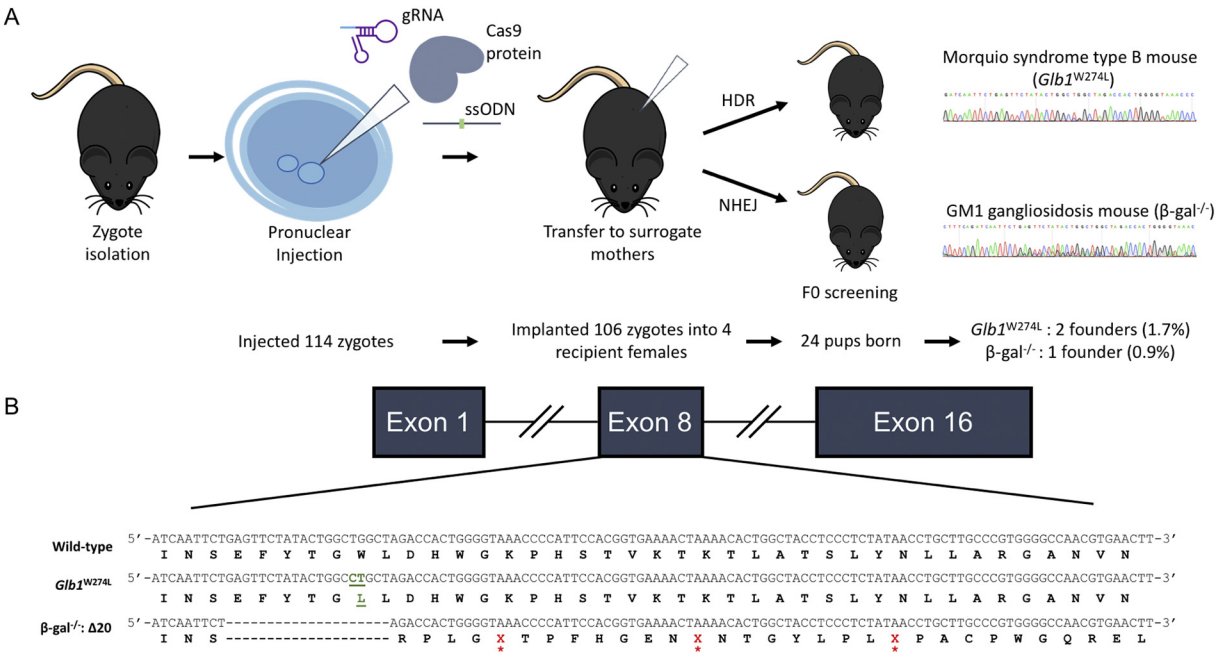

Fig. 1. Generation of β-galactosidase deficient mice. (A) Experimental schematic to develop two models of β-galactosidase deficiency in a single experiment utilizing CRISPR-Cas9 genome editing. (B) Founder animal mutations in exon 8 of β-galactosidase encoding gene *Glb1*. Two mice had 2 bp mutation resulting in tryptophan to leucine substitution commonly found in Morquio syndrome type B patients (*Glb1*^{W274L}, green underlined sequence). Another founder contained a 20 bp deletion (β-gal −/− Δ20; red asterisks denote stop codons introduced by the deletion). (For interpretation of the references to colour in this figure legend, the reader is referred to the web version of this article.)

tissue/10 mL CHAPS solution), cerebral cortex (1 g wet tissue/6 mL CHAPS solution), and hippocampus (1 g wet tissue/10 mL CHAPS solution) in 2% CHAPS solution. Protein precipitation with 200 µL of methanol was performed to extract gangliosides GM1, GA1, GM2, and GM3 from 50 µL of homogenate in the presence of internal standards (GA1 standard converted from N-CD_3-Stearoyl-GM1 (18:0) (Matreya, State College, PA) using methods described in [24]). The 10% study sample extracts from each tissue type were pooled to prepare a quality control (QC) sample for that tissue. QC samples were injected every 5 study samples to monitor the instrument performance. Samples reported have a QC coefficient of variance < 15%.

Sample analysis was performed with a Shimadzu 20AD HPLC system coupled to a 6500QTRAP + mass spectrometer (AB Sciex, Framingham, MA) operated in positive MRM mode. Data processing was conducted with Analyst 1.6.3 (Applied Biosystems). Data were reported as the peak area ratios of the analytes in sample to the corresponding internal standards.

2.6. Mouse behavior analysis

At 6 months of age, mice were subjected to multiple behavior tests to assess neuromotor and neurocognitive function. All behavioral analyses were conducted in the Mouse Behavior Core at the University of Minnesota.

2.6.1. Neuromotor testing

2.6.1.1. Balance beam. The balance beam protocol was adapted from [25,26]. Trials were performed on a 1 m long wooden beam, held 48 cm above the table by a platform on one end (start) and a dark enclosure "safe box" on the other (stop). Before the first trial was conducted each day, the mouse was habituated for 15 s in the safe box. To begin the trial, the mouse was placed on the start platform under an aversive light in a dark room. The latency to cross the beam and enter the enclosure was measured, in addition to the number of hind foot slips that occur while crossing the beam. Each mouse was trained on a square beam (25 mm wide) for three days, with four trials per day. On day four, mice were subjected to two trials on beams of increasing difficulty: 25 mm square beam, followed by 27 mm round beam, and lastly the 15 mm wide square beam. Again, latency to cross and number of hind foot slips were measured. Max trial duration was limited to 60 s.

2.6.1.2. Pole test. The pole test was conducted as previously described with minor modifications [27]. The test began by placing a mouse head-upward on a vertical pole (10 cm in diameter; 55 cm tall) wrapped in athletic tape to assist with grip. Two measurements were taken: Latency to rotate body to face downward was measured, in addition to total time to descend the pole and place all 4 paws on the base of the apparatus inside of the cage, with a maximum test duration of 60 s. If a mouse failed to make the initial rotation to face downward, 60 s was recorded for both the turn and total time to descend. If the mouse fell from the pole during the testing time, it was placed back at the initial starting point while the time continued until 60 s. Mice were subjected to a single trial.

2.6.1.3. Rotarod. Rotarod analysis was conducted on an accelerating rotarod (Ugo Basile, Comerio, Italy), using an adapted protocol described previously [28]. Briefly, mice were tested for three consecutive days, undergoing four trials per day, with a minimum inter-trial duration of 30 min. Testing was done on a rotarod programmed to accelerate from 5 to 50 rpm over a max trial duration of 300 s. 3–5 mice were placed on the divided rod simultaneously and the apparatus' counter was started. The trial was considered complete when 1) the mouse fell off the rotarod and stopped the counter, 2) the mouse completes two consecutive rotations by holding on to the rod without walking, or 3) when 300 s elapsed.

2.6.1.4. Inverted screen. Inverted screen testing [29] was completed utilizing a wire mesh apparatus, approximately 25 cm × 25 cm with 25 mm^2 square openings, placed approximately 30 cm over a cushioned surface. Testing began by placing the mouse on the wire mesh, which was then inverted until the animal was completely upside down. Latency to fall was measured for a max trial duration of 60 s. Mice

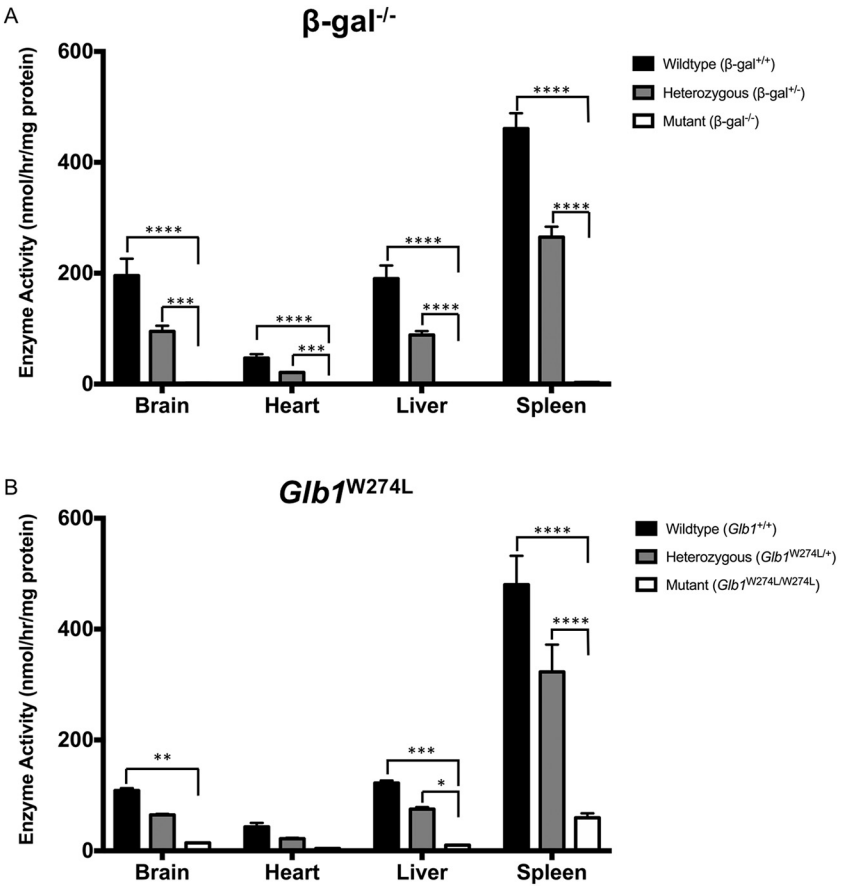

Fig. 2. β-galactosidase enzyme activity. (A) Enzyme activity in β-gal$^{-/-}$ mouse brain, heart, liver, and spleen (wildtype $n = 5$, heterozygous $n = 9$, mutant $n = 7$). (B) Enzyme activity in *Gbl1*^{W274L} brain, heart, liver, and spleen (wildtype $n = 3$, heterozygous n = 3, mutant $n = 4$). Data are mean ± SEM. $^{*}p \leq 0.05$, $^{**}p \leq 0.01$, $^{***}p \leq 0.001$, $^{****}p \leq 0.0001$ when comparing mutant mice to wildtype and heterozygous mice.

were subjected to 3 trials, with a minimum of 15-min resting period between trials.

2.6.2. Neurocognitive testing

2.6.2.1. Barnes maze. The Barnes maze [30] was conducted on an elevated circular platform, 36 in. in diameter, with 20 equally spaced holes around its perimeter. All of the holes on the platform were blocked except for one, which contained an opening to an escape box. The apparatus was placed directly under a bright light source that served as an aversive stimulus for the mouse to escape the platform. Visual cues were placed on each of the walls that act as navigational cues for the mouse. Mice were trained on the Barnes maze for 4 days, with each mouse subjected to 4 trials per day, with a max of 3 min per trial, and a minimum of 30 min between trials. Data was collected utilizing the ANY-Maze software (Stoelting Co, Wood Dale, IL).

2.6.2.2. Spontaneous alternation T-maze. The spontaneous alternation T-maze test [31] was utilized to analyze the spatial and working memory of the animals utilizing a maze consisting of three arms. The starting arm of the maze contained a small compartment which was separated from the rest of the maze by a guillotine door. The two choice arms of the maze contained different visual cues on the end walls for the mouse to utilize. Testing was done in a dark room with the maze lit by utilizing a portable canopy light over the choice arms. A mouse was placed in the start chamber for 5 s, after which the guillotine door is opened and the mouse was allowed to explore the maze and freely choose either choice arm. Once the animal's body completely entered the choice arm, a removable partition was placed behind the mouse, blocking the animal within the chosen arm for 15 s. This first trial is referred to as the free choice trial. The animal was then placed back into the start box for 5 s and the test was repeated, for a total of 11 trials (1 free choice, 10 choice trials). Once all trials were completed, the percent of correct alternations was calculated. On the following day, the experiment was repeated and the average percentage of correct alternations was calculated and reported.

2.7. Statistical analysis

GraphPad Prism 7 (v. 7.0a, GraphPad Software, Inc) was used to perform all statistical analyses. For all experiments, wildtype, heterozygous, and mutant groups were compared by one-way or two-way ANOVA followed by Tukey's multiple comparisons test. All values presented as mean ± SEM.

3. Results

3.1. Generation of β-galactosidase deficient mouse models

A total of 106 blastocysts were implanted into 4 pseudopregnant female mice, yielding 24 live pups (Fig. 1A). PCR amplification and sequencing of the targeted site showed that three of the 24 mice contained potential mutations of interest. Two founder mice had undergone homology-directed repair to generate the targeted 2 bp missense mutation of interest at position 274 (*Glb1*^{W274L}, Fig. 1B). Additionally, one mouse had undergone non-homologous end joining, which resulted in a 20 bp deletion within exon 8, yielding 3 premature stop codons in addition to deleting the catalytic nucleophile of β-galactosidase, the glutamic acid at position 269 (*Glb1*^{Glu269} in mice; *Glb1*^{Glu268} in humans) [32] (β-gal$^{-/-}$Δ20, Fig. 1B).

One potential pitfall of CRISPR-Cas9 genome editing is off-target cutting by the Cas9 nuclease. To predict potential off-target sites of Cas9 DNA cleavage, the CCTOP algorithm [33] was used. Sites of interest were determined by gRNA sequence homology near a potential PAM sequence. Ten loci were sequenced, 5 containing the NGG PAM

sequence and 5 with a NAG PAM sequence (Supplemental Table 1). These sequencing results showed that the potential off-target sites were unedited (data not shown).

In β-gal$^{-/-}$ mice, it was predicted that the deletion of the catalytic nucleophile and introduction of premature stop codons would result in loss of β-gal enzyme activity. As expected, β-gal enzyme activity in β-gal$^{-/-}$ mice was negligible in the brain (1.9 ± 0.2 nmol/h/mg of protein), heart (0.6 ± 0.5), liver (0.6 ± 0.3), and spleen (3.3 ± 1.0) in comparison to wildtype (brain, 195.8 ± 30.2; heart, 47.1 ± 7.0; liver, 190.3 ± 23.5; and spleen, 460.9 ± 27.7) and heterozygous mice (brain, 95 ± 10.1; heart, 20.9 ± 0.9; liver, 88.7 ± 6.9; and spleen, 264.1 ± 18.6) (Fig. 2A).

Similar to Morquio syndrome type B patients with the *GLB1*^{W273L} mutation, homozygous *Glb1*^{W274L} mutant mice had residual β-gal enzyme activity. Offspring from both founders had comparable enzyme activity levels. In the brain, β-gal enzyme activity in homozygous *Glb1*^{W274L} mutant mice (14.5 ± 0.6 nmol/h/mg of protein) was 13.3% of wildtype activity (108.9 ± 4.0). Similarly, in the heart (4.2 ± 0.4), liver (10.3 ± 0.8), and spleen (59.8 ± 8.1) of *Glb1*^{W274L} mice, β-gal enzyme activity was 9.8%, 8.4%, and 12.4%, of wildtype activity, respectively (heart, 43.2 ± 7.1; liver, 122.5 ± 4.4; and spleen, 480.3 ± 52.0). As expected, carriers of the *Glb1*^{W274L} mutation have an intermediate β-gal enzyme activity (brain, 65.0 ± 1.8; heart, 22.0 ± 1.5; liver, 75.3 ± 3.5; and spleen, 322.9 ± 49.2) (Fig. 2B).

Male and female mice from both the *Glb1*^{W274L} and β-gal$^{-/-}$ lines are fertile and produce normal litters. However, after 5 months of age, β-gal$^{-/-}$ mice cease breeding. Whether this is due to neurological symptom onset or another physiological reason has yet to be tested.

3.2. Appearance and survival

At birth, both *Glb1*^{W274L} and β-gal$^{-/-}$ mice were indistinguishable from their littermates. At 4 months of age, β-gal$^{-/-}$ mice began showing gait disturbance in their hind limbs, followed by body tremors and ataxia around 5 months. While heterozygous and wildtype female mice continued to gain weight for the first year of life, female β-gal$^{-/-}$ mice peaked at 25.3 ± 0.4 g at approximately 33 weeks of age (~7.5 months), after which their weight declined rapidly (Fig. 3A). Surprisingly, male β-gal$^{-/-}$ mice became significantly heavier than their littermates at 25 weeks of age (45.3 ± 1.2 g compared to wildtype, 40.0 ± 1.2 g and heterozygous, 38.0 ± 0.9 g) (Fig. 3B). Following this peak weight, male β-gal$^{-/-}$ mice began to lose weight rapidly, similar to female β-gal$^{-/-}$ mice. This decline in weight coincided with the overall decline in health of the β-gal$^{-/-}$ mice.

Similar to the previously published mouse models of GM1-gangliosidosis, at 6 months of age, β-gal$^{-/-}$ mice displayed a severe neurological disease phenotype. 6-month-old female (Supplementary Movie 1) and male (Supplementary Movie 2) β-gal$^{-/-}$ mice had an ataxic gait, with a stiff, curled tail, as if it were being used for balance. At 9 months of age, both female (Supplementary Movie 3) and male (Supplementary Movie 4) β-gal$^{-/-}$ mice displayed a severe neurological deterioration, manifesting as physical instability and labored ambulation. As the disease progressed, neurological symptoms of β-gal$^{-/-}$ mice significantly worsened, leading to a loss of function in their forelimbs and hindlimbs and subsequently became paralyzed.

In agreement with previous mouse models of GM1-gangliosidosis, β-gal$^{-/-}$ mice had a significantly shortened lifespan compared to wildtype and heterozygous animals, which have an average lifespan over 2 years. In females, the lifespan of β-gal$^{-/-}$ mice was 264.4 ± 34.9 days (mean ± standard deviation) (Fig. 3C). Likewise, the lifespan of male β-gal$^{-/-}$ mice was 265.2 ± 21.2 days (Fig. 3D). One wildtype mouse required euthanasia at 350 days due to injuries sustained from fighting.

In contrast, *Glb1*^{W274L} mice displayed no observable phenotype over the course of one year. Detailed histopathology examination of 8-week old mice showed no abnormalities. Skeletal X-rays showed no morphological abnormalities, and quantification of keratan sulfate in plasma was not increased compared to control mice (data not shown). Additionally, both female (Fig. 3E) and male (Fig. 3F) mice weights did not differ from wildtype and heterozygous mice. Not surprisingly, *Glb1*^{W274L} mice showed no increase in mortality (Fig. 3G-H). Because of the lack of a visible phenotype, no further characterization of the *Glb1*^{W274L} line will be discussed here.

3.3. Ganglioside accumulation in β-gal$^{-/-}$ mouse brains

To determine whether the deficiency in β-gal enzyme activity resulted in ganglioside accumulation, high-performance liquid chromatography, tandem mass spectrometry was implemented to quantify GM1 and GA1 gangliosides in β-gal$^{-/-}$ brains. As the 18-carbon atom sphingosine chain length is the most abundant GM1 and GA1 ganglioside [34], this was chosen as the biomarker for quantification. In the cerebral cortex, there was a 1.6-fold increase in GM1 ganglioside compared to control animals, where GA1 ganglioside was increased 2.5-fold (Fig. 4A). In the cerebellum GM1 and GA1 ganglioside content was 4.0-fold and 7.3-fold higher than controls, respectively (Fig. 4B). Further, in the hippocampus, GM1 ganglioside was 2.2-fold higher than controls, in addition to a 3.6-fold increase in GA1 ganglioside (Fig. 4C).

In addition to quantifying the primary substrate of β-gal, the secondary accumulation of GM2 and GM3 ganglioside was measured. In all three brain regions analyzed, secondary ganglioside accumulation was significantly increased, except in the case of GM3 ganglioside in the cerebellum. In the cerebral cortex, GM2 ganglioside accumulation was 2.6-fold higher than wildtype, while there was a 4.5-fold increase of GM3 ganglioside (Fig. 4A). In the cerebellum, GM2 ganglioside content was 1.5-fold higher than controls and GM3 ganglioside was increased 1.8-fold (Fig. 4B). In the hippocampus, the amount of GM2 ganglioside was increased 2.6-fold and GM3 ganglioside was increased 2.4-fold (Fig. 4C).

Histopathological examination of the CNS in β-gal$^{-/-}$ mice revealed a striking and widespread marked swelling and enlargement of neurons with pale, finely granular to foamy cytoplasm that occasionally displaced the nucleus to the periphery. Neuronal cytoplasmic vacuolation was variable, and was observed within the cerebral cortex, thalamus, Cornu Ammonis (mainly CA3) of the hippocampus, brainstem nuclei, cerebellum (Purkinje cells and deep cerebellar nuclei), and spinal cord (ventral and dorsal spinal horns) (Fig. 5). These findings are consistent with the CNS findings for β-gal$^{-/-}$ mice described previously [11,12], are characteristic findings in the of the lysosomal disease GM1-gangliosidosis in the brain, and were absent in control mice. In addition, although negative with PAS, toluidine blue, and alcian blue stains, affected neurons stained positively for Luxol fast blue (Fig. 6), as has been described in several animal models of gangliosidoses [35,36]. In addition to the CNS findings, we also observed cellular enlargement with cytoplasmic vacuolation involving hepatocytes of the liver, acinar cells of the pancreas, and enterocytes of the intestine (Supplementary Fig. 1).

3.4. Severe neuromotor deficiencies in β-gal$^{-/-}$ mice

At 6 months of age, neuromotor function was tested using several behavioral tests. First, β-gal$^{-/-}$ mice were subjected to the balance beam. Both female (Fig. 7A) and male (Fig. 7B) β-gal$^{-/-}$ mice took significantly longer to cross the 25 mm square beam on all 4 test days compared to heterozygous and wildtype mice. In addition to a longer latency to cross the beam, β-gal$^{-/-}$ mice had significantly more hindlimb foot slips while crossing the beam (Fig. 7C & D). On Day 4, animals were subjected to beams of increasing difficulty. Again, β-gal$^{-/-}$ mice took significantly longer to cross the beams compared to control mice (Fig. 7E & F) and the number of foot slips was elevated (Fig. 7G & H), indicating that β-gal$^{-/-}$ mice had a severe motor coordination deficit.

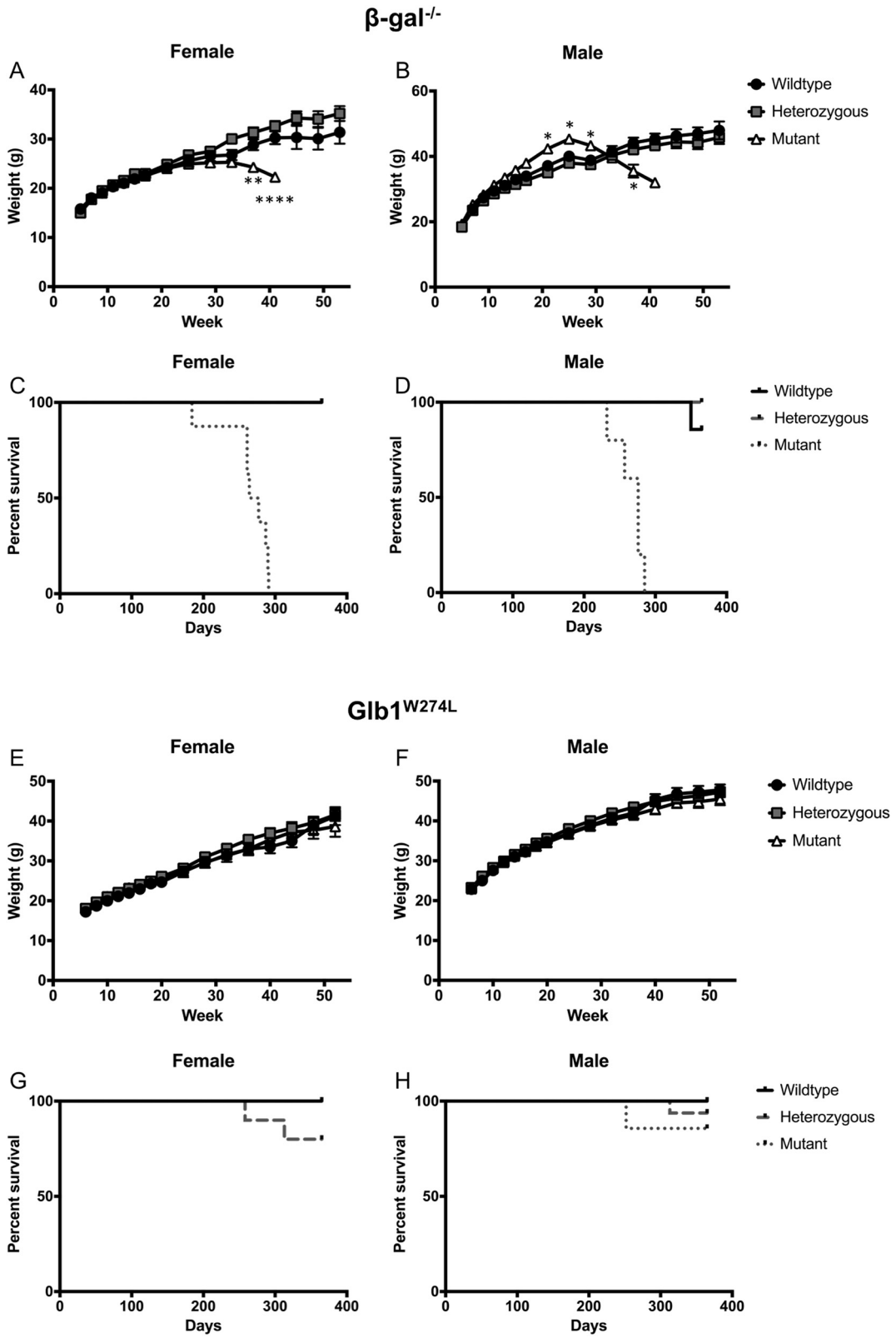

Fig. 3. Weight and survival analysis of β-galactosidase deficient mice. (A and B) Weight of β-gal$^{-/-}$ mice over one year ($n > 5$ for each group, except mutant males at timepoint week 41 where $n = 1$). (C and D) Kaplan-Meier survival curve of β-gal$^{-/-}$ mice ($n = 5$–8 for each group). (E and F) Weight of *Glb1*^{W274L} mice over one year ($n > 6$ for each group). (G and H) Kaplan-Meier survival curve of *Glb1*^{W274L} mice ($n = 7$–16 for each group). Weight data are mean ± SEM. *$p \leq 0.05$, **$p \leq 0.01$, ****$p \leq 0.0001$. β-gal$^{-/-}$ survival significantly reduced ****p ≤ 0.0001.

The second test of neuromotor function was the accelerating rotarod, which tests motor coordination and motor learning. Over the 3 days of trials, the latency to fall of both female (Fig. 8A) and male (Fig. 8B) β-gal$^{-/-}$ mice was significantly lower than heterozygous and wildtype mice. Additionally, β-gal$^{-/-}$ showed an inability to learn to stay on the rotarod between trial days, whereas control animals

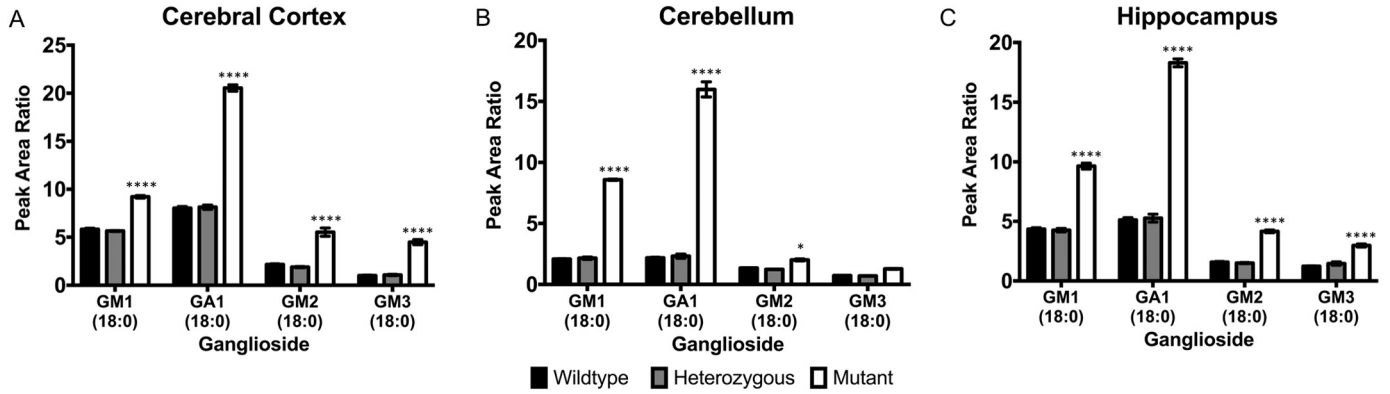

Fig. 4. Ganglioside quantification in brain tissue of β-gal$^{-/-}$ mice. GM1, GA1, GM2, and GM3 gangliosides accumulation in the (A) cerebral cortex, (B), cerebellum, and (C) hippocampus of mice ($n = 3$ for each group) were measured using high performance liquid chromatography tandem-mass spectrometry. Data are reported as the peak area ratios of analytes in the sample to the corresponding internal standard. Data are mean ± SEM. *$p \leq 0.05$, ****$p \leq 0.0001$.

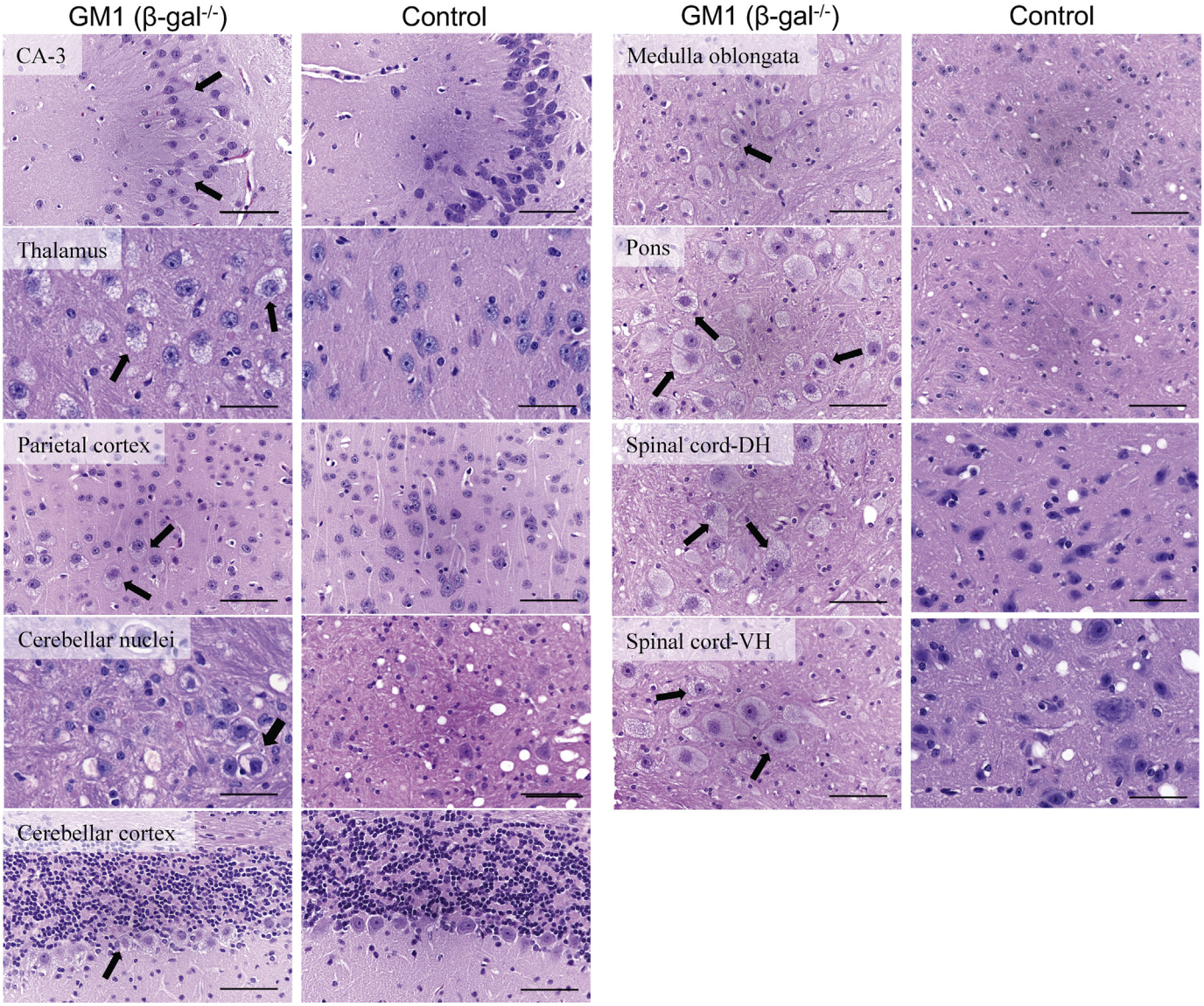

Fig. 5. Widespread marked enlargement of neurons with cytoplasmic vacuolation (reflecting significant accumulation of storage material) in the central nervous system of β-gal$^{-/-}$ mice. Hematoxylin and eosin staining of brain and spinal cord of β-gal$^{-/-}$ and control mice. Brain and spinal cord (β-gal$^{-/-}$): objective x40, scale bar indicates 30 μm; spinal cord control: objective x60, scale bar indicates 20 μm.

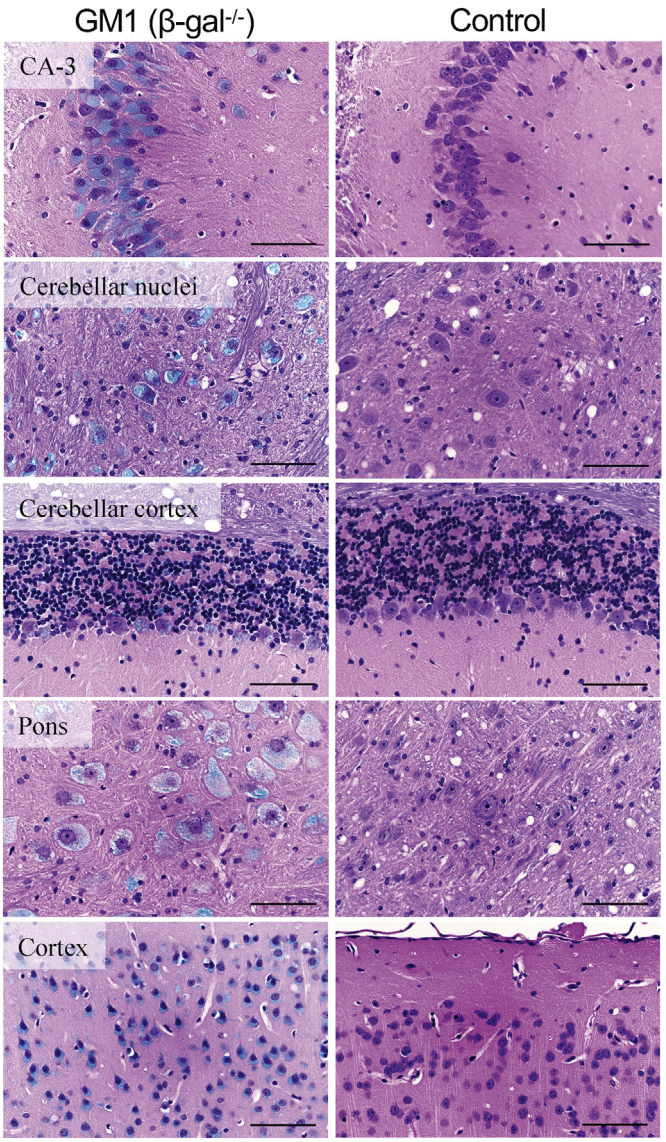

Fig. 6. Histopathological images of Luxol fast blue-stained brain tissue from β-gal$^{-/-}$ mice compared with control mice. Neurons of β-gal$^{-/-}$ mice are enlarged/swollen, and contain abundant intracytoplasmic, granular, Luxol fast blue positive material, with occasional nuclear peripheralization. Objective x40, scale bar indicates 30 μm.

improved their latency to fall on subsequent days. Overall, this test supported the finding that β-gal$^{-/-}$ mice have severe motor coordination deficiencies, in addition to a lack of motor learning.

Thirdly, the pole test was utilized to assess bradykinesia, typically observed in other CNS diseases such as Parkinson's disease (reviewed in [37]). In both β-gal$^{-/-}$ females (Fig. 8C) and males (Fig. 8D), the inversion time was significantly longer than heterozygous and wildtype mice. Similar results were seen in the total descent time. Female (Fig. 8E) and male (Fig. 8F) β-gal$^{-/-}$ mice took significantly longer, or could not complete the initial inversion task to descend the pole, compared to heterozygous and wildtype mice, who could complete the task with relative ease.

The last test used to analyze neuromotor function was the inverted screen test to measure grip strength. The latency to fall of female β-gal$^{-/-}$ mice averaged 17.6 ± 3.7 s, where heterozygous and wildtype mice could remain on the inverted screen for 59.1 ± 0.6 s and 57.4 ± 1.2 s, respectively (Fig. 8G). Male β-gal$^{-/-}$ mice showed a similar significant loss of grip strength, only being able to stay on the screen for 3.4 ± 0.5 s, compared to 53.4 ± 2.9 s in heterozygous mice, and 49.9 ± 2.4 s in wildtype mice (Fig. 8H). In summation, the results of this test and the extensive behavior tests of motor function showed that β-gal$^{-/-}$ mice have severe neuromotor impairments.

3.5. Impaired neurocognitive function of β-gal$^{-/-}$ mice

Previous studies from our group have shown that cognition is significantly impaired in mouse models of other lysosomal diseases [38,39]. To test the spatial reference memory of β-gal$^{-/-}$ animals, the Barnes maze was implemented. Over the course of 4 days of testing, the latency to escape the platform of wildtype and heterozygous animals progressively decreased in females from 158.7 ± 9.6 and 159.9 ± 10.0 s on Day 1 to 42.4 ± 5.4 and 35.1 ± 5.0 s on Day 4 (Fig. 9A). Similarly, in males, the latency to escape decreased from 176.9 ± 2.4 s in wildtype and 180 s in heterozygous mice on Day 1 to 38.2 ± 2.5 s and 42.0 ± 10.8 s on Day 4 (Fig. 9B). These results indicate a normal cognitive function. In comparison, the latency to escape of female and male β-gal$^{-/-}$ mice latency to escape decreased from 180 s for both groups to 177.3 ± 1.8 s and 175.3 ± 4.8 s, respectively. The absence of a decrease in latency to escape suggested that β-gal$^{-/-}$ mice have a learning disability and impaired spatial reference memory.

Additionally, the spatial working memory of β-gal$^{-/-}$ animals was tested using the spontaneous alternating T-maze. This test utilizes the normal tendencies of mice to explore a new environment. If an animal's cognition is impaired, mice will not alternate between arms on subsequent trials, resulting in a random pattern of arm choices (≤50% successful alternation). In this test, female wildtype and heterozygous mice successfully alternated 72.9 ± 2.4% and 75.0 ± 1.9% of the trials, while β-gal$^{-/-}$ mice correctly alternated 47.9 ± 5.9% of the time (Fig. 9C). Similarly, male wildtype and heterozygous mice successfully alternated 74.3 ± 2.8% and 68.8 ± 1.8% of the trials, where β-gal$^{-/-}$ mice correctly alternated 42.0 ± 8.5% of the trials (Fig. 9D). These results suggested the decision of β-gal$^{-/-}$ mice was random, indicating a spatial working memory deficiency.

4. Discussion

β-galactosidase is a unique lysosomal hydrolase, in that when it is deficient, depending on where the mutation is located in the *GLB1* gene and what effect it has on β-gal enzyme activity, it is responsible for two distinct lysosomal diseases: one affecting the central nervous system (GM1-gangliosidosis), and another affecting the skeletal system (Morquio syndrome type B). Recently, our group applied bioinformatic tools to investigate the structure of the β-gal enzyme and provided important inferences about why mutations in one gene can lead to two different diseases [40]. In this paper, we describe two novel murine models of β-galactosidase deficiencies that were developed by using CRISPR-Cas9 genome editing in a single experiment. By utilizing a donor oligonucleotide, homology-directed DNA repair was promoted to introduce a 2 bp substitution commonly found in patients suffering from Morquio syndrome type B [4–7,9]. This mutation, *GLB1*^{W273L}, occurs in a highly conserved region of the *GLB1* gene. The tryptophan residue is predicted to be important for the secondary structure of β-galactosidase [32], and when mutated, reduces the ability of the enzyme to catabolize keratan sulfate, resulting in Morquio syndrome type B. Here we have described the introduction of this 2 bp mutation into mice (*Glb1*^{W274L}). Similar to what has been described in Morquio syndrome type B patients, the presence of a β-gal enzyme deficiency was observed. While residual β-gal enzyme activity was present, it ranged between 8.4 and 13.3% of wildtype levels, depending upon the tissue assayed. However, even though β-gal enzyme activity is diminished, after one year, *Glb1*^{W274L} mice show no observable skeletal phenotype. An explanation of this observation may be due to the absence of keratan sulfate in skeletal tissues of mice [41]. However, keratan sulfate-containing proteoglycans are present within the cornea of the mouse,

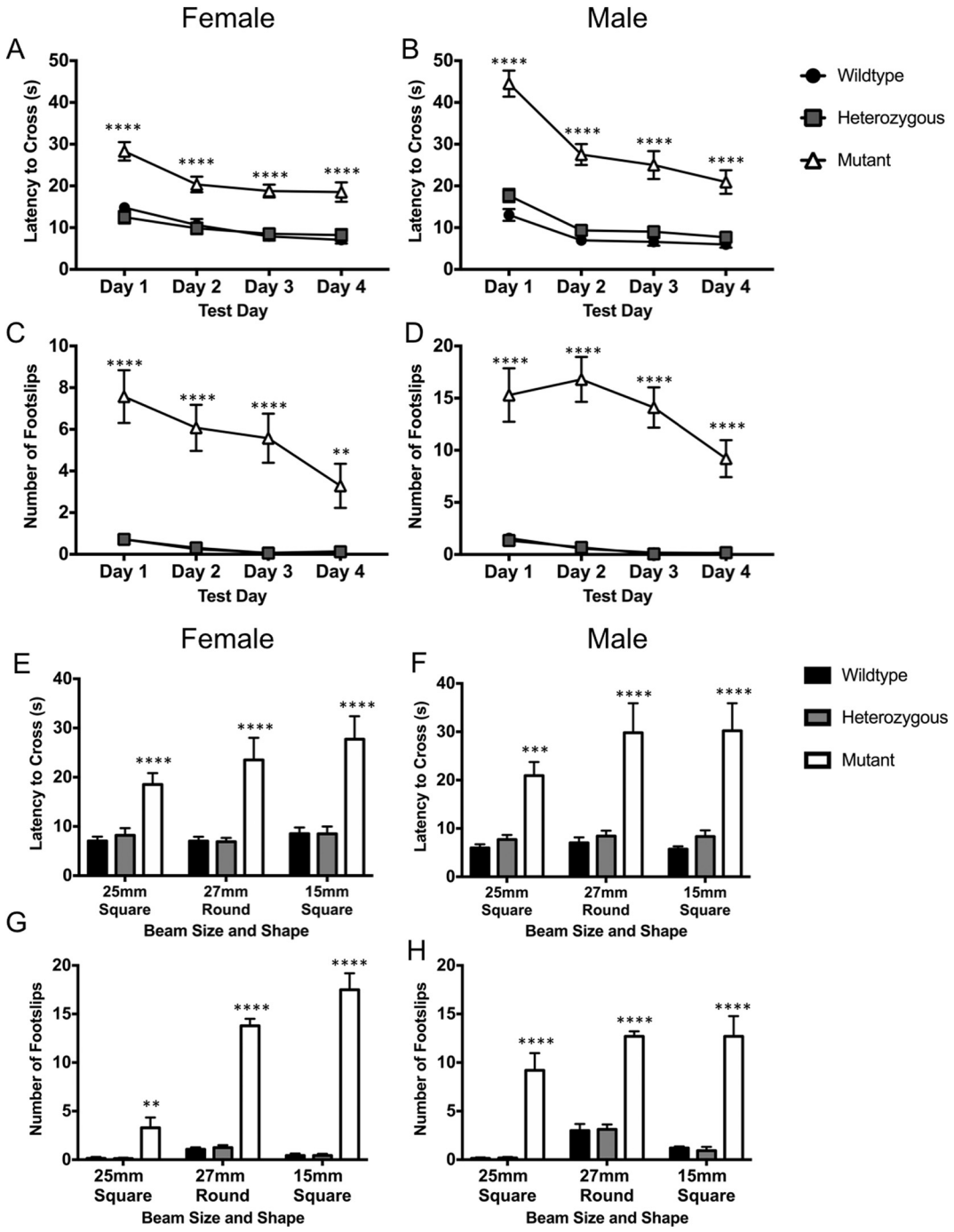

Fig. 7. Impaired balance and motor coordination β-gal$^{-/-}$ mice. At 6 months of age, β-gal$^{-/-}$ mice were tested on a balance beam. (A and B) Latency to cross beam and (C and D) number of hindlimb foot slips while crossing the beam. (E and F) Latency to cross beams of increasing difficulty and (G and H) number of hindlimb foot slips while crossing the beam on test day (n = 5–8 for each group). Data are mean ± SEM. $^{**}p \leq 0.01$, $^{***}p \leq 0.001$, $^{****}p \leq 0.0001$.

beginning around postnatal day 20 [42,43]. Further studies will have to be conducted to determine whether the reduction in β-gal activity results in a corneal phenotype.

In the second model, a 20 bp deletion was introduced into exon 8 of the β-gal encoding gene as a result of non-homologous end joining DNA repair. This mutation resulted in the deletion of a highly conserved region of DNA, including the catalytic nucleophile (*Glb1*^{Glu269}) of the β-gal enzyme. While there have been no patients with a mutation resulting in a loss of the catalytic nucleophile described, this mutation is predicted to result in both Morquio syndrome type B and GM1-gangliosidosis, as a catabolic reaction could not occur [44]. In our mouse model, the 20 bp mutation results in a complete loss of β-gal enzyme activity and subsequent accumulation of the primary storage materials GM1 ganglioside and its asialo derivative GA1 ganglioside in the central nervous system as shown by histopathology and ganglioside quantification. An alternative pathway of GM1 ganglioside catabolism exists apart from GM1 ganglioside to GA1 ganglioside conversion by neuraminidase. In the presence of ceramide deacylase, GM1 ganglioside can be converted to lyso-GM1, which has been shown to be elevated in patients with GM1-gangliosidosis [45]. It is believed that lyso-GM1 is also neuropathic, similar to other toxic lysosphingolipids like galactosylsphingosine and glucosylsphingosine in Krabbe and Gaucher diseases, respectively. Further, secondary accumulation of glycosphingolipids such as glucosylceramide, lactosylceramide, GM2, GM3,

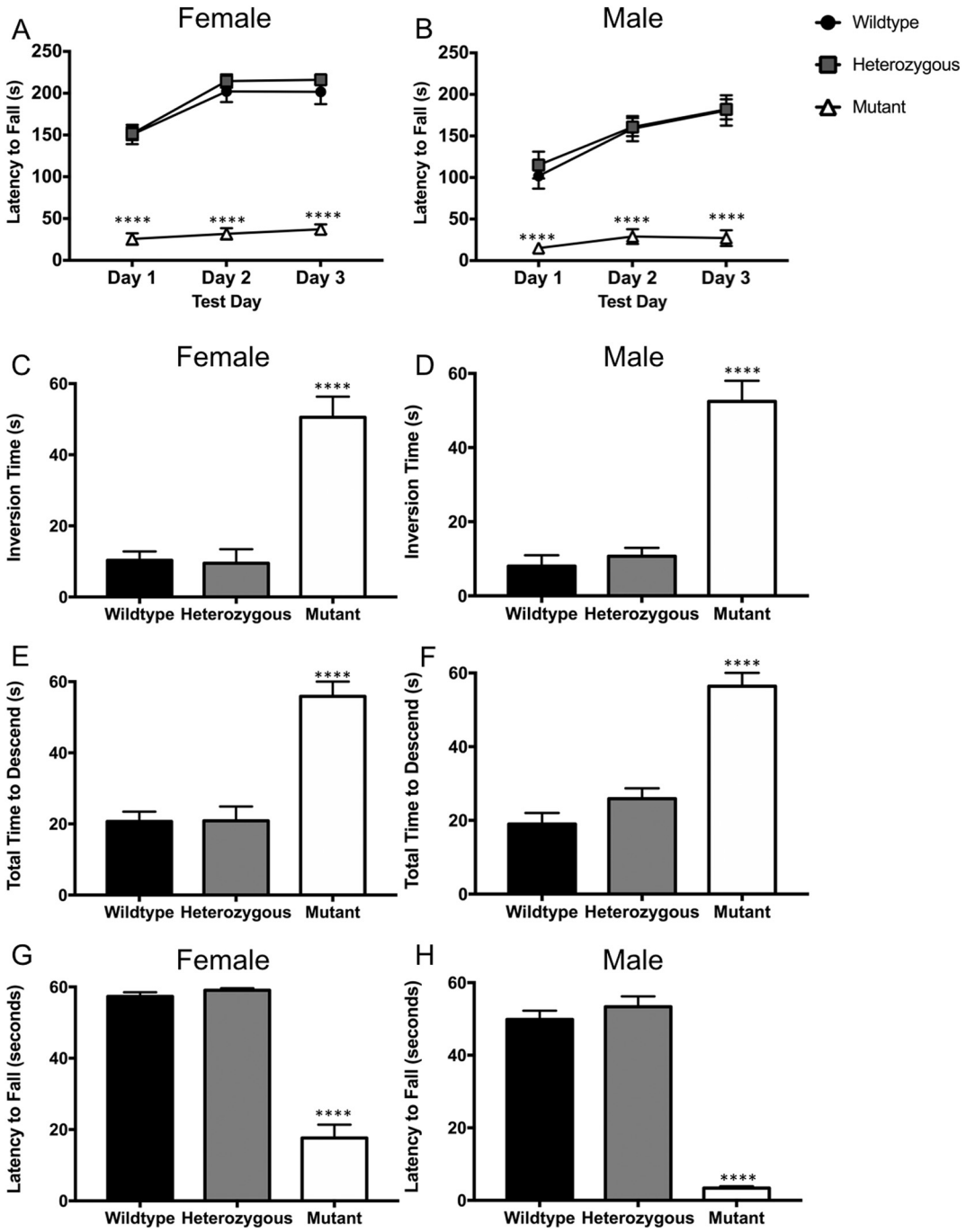

Fig. 8. Significant motor deficiency and loss of strength in β-gal$^{-/-}$ mice. (A and B) Rotarod testing (n = 5–8 for each group), (C—F) pole test (n = 5–8 for each group), and (G and H) inverted screen testing (n = 5–11 for each group) carried out at 6 months of age. Data are mean ± SEM. ****$p \leq 0.0001$.

and GD1a gangliosides in GM1-gangliosidosis patients has been reported [46–48]. In the β-gal$^{-/-}$ mouse model reported here, a significant secondary accumulation of GM2 and GM3 gangliosides in the brain was observed. Overall, the accumulation of gangliosides resulted in progressive severe neuromotor decline, similar to what was previously described [13,14]. Additionally, β-gal$^{-/-}$ mice showed a severe neurocognitive impairment not previously described. Further, these impairments led β-gal$^{-/-}$ mice to become sick and lose a significant amount of weight beginning around 29 weeks in females and 25 weeks in males. Eventually, β-gal$^{-/-}$ mice succumbed to the disease by 10 months of age.

Prior to this publication, the only mouse models of β-galactosidase deficiency that existed were those generated using the time-consuming ES cell approach that utilizes the introduction of an exogenous neomycin resistance gene sequence to interrupt *Glb1* gene expression. However, their use in β-galactosidase deficiency studies is likely limited to studying enzyme replacement therapies [49] or gene therapies [13,14,50,51]. However, most patients who suffer from GM1-gangliosidosis or Morquio syndrome type B do not have a complete β-gal enzyme deficiency. In reality, many patients with juvenile or adult onset GM1-gangliosidosis or Morquio syndrome type B have a single amino acid substitution that affects the secondary or tertiary structure of β-gal, reducing its catalytic activity. With the creation of the *Glb1*^{W274L} model described in this manuscript, the ability to test enzyme-stabilizing small molecules becomes a possibility. A second potential limitation of the previous models of GM1-gangliosidosis is the

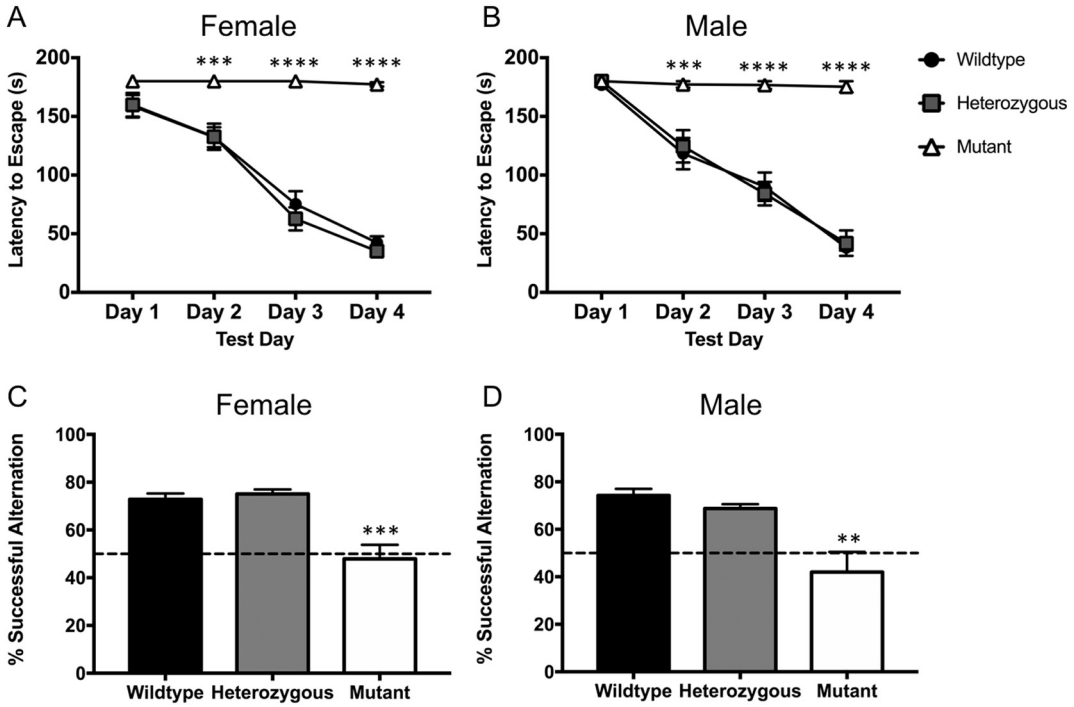

Fig. 9. Severe neurocognitive dysfunction in β-gal$^{-/-}$ mice. (A and B) Barnes maze (n = 5–11 for each group) and (C and D) spontaneous alternating T-maze (n = 5–8 for each group) in 6-month-old mice. Dashed line represents 50%. Data are mean ± SEM. $^{**}p \leq 0.01$, $^{***}p \leq 0.001$, $^{****}p \leq 0.0001$.

possibility of a random mutation arising in the modified *Glb1* locus that results in the introduction of a novel splice site, causing skipping of the exon encoding the neomycin gene. The result of this would be a shortened amino acid sequence, but could potentially yield a catalytically active β-gal enzyme. In the model described here, the possibility of this occurring is nonexistent, because the amino acid responsible for the catalytic activity of the enzyme (*Glb1*^{Glu269}) has been removed. One potential limitation of the models described here, though, could be that they were derived on a pure C57BL/6J background, thus the results of experiments conducted on these animals may not be recapitulated in other genetically different strains of mice. However, it is postulated that this will not be an issue due to the fact that the previously described models developed on alternative genetic backgrounds show similar phenotypes to those described here. Future studies, including proteomics [52] and metabolomics [53], could be applied to further characterize these models and study the etiology of these diseases.

In conclusion, we have described the use of CRISPR-Cas9 genome editing to develop two new models of β-galactosidase deficiency. The first model recapitulates the enzyme deficiency observed in Morquio syndrome type B patients, which is the first description of a mouse model to have residual β-gal enzyme activity. In the second model, many characteristics of infantile GM1-gangliosidosis are displayed. Overall, these mice will be essential for the future development and testing of novel therapies for Morquio syndrome type B and GM1-gangliosidosis.

Supplementary data to this article can be found online at https://doi.org/10.1016/j.ymgme.2018.11.002.

Acknowledgements

Quantification of gangliosides was supported through funding from the National Tay-Sachs & Allied Diseases Association, Inc. (NTSAD). We thank Dr. Shunji Tomatsu at the University of Delaware for providing his expertise in quantifying plasma keratan sulfate. Generation of β-galactosidase deficient mice was performed at the Animal Models Core Facility at the University of North Carolina at Chapel Hill under the direction of Dr. Dale Cowley.

References

[1] J.S. O'Brien, M.B. Stern, B.H. Landing, J.K. O'Brien, G.N. Donnell, Generalized gangliosidosis, another inborn error of ganglioside metabolism? Am. J. Dis. Child. 109 (1965) 338–346.
[2] K. Suzuki, Cerebral GM1-gangliosidosis: chemical pathology of visceral organs, Science 159 (1968) 1471–1472.
[3] Y. Suzuki, E. Nanba, J. Matsuda, K. Higaki, A. Oshima, Beta-galactosidase deficiency (beta-galactosidosis): GM1 gangliosidosis and Morquio B disease, in: C.R. Scriver, A.L. Beaudet, W.S. Sly, D. Valle (Eds.), The Metabolic and Molecular Basis of Inherited Disease, McGraw-Hill, New York, 2001, pp. 3775–3809.
[4] A. Oshima, K. Yoshida, M. Shimmoto, Y. Fukuhara, H. Sakuraba, Y. Suzuki, Human β-galactosidase gene mutations in morquio B, Dis. Am. J. Hum. Genet. 49 (1991) 1091–1093.
[5] D. Hofer, K. Paul, K. Fantur, M. Beck, F. Burger, C. Caillaud, K. Fumic, J. Ledvinova, A. Lugowska, H. Michelakakis, B. Radeva, U. Ramaswami, B. Plecko, E. Paschke, GM1 gangliosidosis and Morquio B disease: expression analysis of missense mutations affecting the catalytic site of acid beta-galactosidase, Hum. Mutat. 30 (2009) 1214–1221.
[6] K. Fantur, D. Hofer, G. Schitter, A.J. Steiner, B.M. Pabst, T.M. Wrodnigg, A.E. Stutz, E. Paschke, DLHex-DGJ, a novel derivative of 1-deoxygalactonojirimycin with pharmacological chaperone activity in human G(M1)-gangliosidosis fibroblasts, Mol. Genet. Metab. 100 (2010) 262–268.
[7] Y. Tatano, N. Takeuchi, J. Kuwahara, H. Sakuraba, T. Takahashi, G. Takada, K. Itoh, Elastogenesis in cultured dermal fibroblasts from patients with lysosomal β-galactosidase, protective protein/cathepsin A and neuraminidase-1 deficiencies, J. Med. Investig. 53 (2006) 103–112.
[8] R. Santamaria, A. Chabas, J.W. Callahan, D. Grinberg, L. Vilageliu, Expression and characterization of 14 GLB1 mutant alleles found in GM1-gangliosidosis and Morquio B patients, J. Lipid Res. 48 (2007) 2275–2282.
[9] E. Paschke, I. Milos, H. Kreimer-Erlacher, G. Hoefler, M. Beck, M. Hoeltzenbein, W. Kleijer, T. Levade, H. Michelakakis, R. B, Mutation analyses in 17 patients with deficiency in acid β-galactosidase: three novel point mutations and high correlation of mutation W273L with Morquio disease type B, Hum. Genet. 109 (2001) 159–166.
[10] J.S. O'Brien, E. Giedion, A. Giedion, U. Wiessmann, N. Herschkowitz, C. Meier, J. Leroy, Sponyloepiphyseal dysplasia, corneal clouding, normal intelligence and acid β-galactosidase deficiency, Clin. Genet. 9 (1976) 495–504.
[11] C.N. Hahn, M. del Pilar Martin, M. Schröder, M.T. Vanier, Y. Hara, K. Suzuki, K. Suzuki, A. D'Azzo, Generalized CNS disease and massive GM1-ganglioside accumulation in mice defective in lysosomal acid β-galactosidase, Hum. Mol. Genet. 6 (1997) 205–211.
[12] J. Matsuda, O. Suzuki, A. Oshima, A. Ogura, Y. Noguchi, Y. Yamamoto, T. Asano, K. Takimoto, K. Sukegawa, Y. Suzuki, M. Naiki, β-Galactosidase-deficient mouse as an animal model for GM1-gangliosidosis, Glycoconj. J. 14 (1997) 729–736.
[13] R.C. Baek, M.L. Broekman, S.G. Leroy, L.A. Tierney, M.A. Sandberg, A. D'Azzo, T.N. Seyfried, M. Sena-Esteves, AAV-mediated gene delivery in adult GM1-gangliosidosis mice corrects lysosomal storage in CNS and improves survival, PLoS One

5 (2010) e13468.
[14] C.M. Weismann, J. Ferreira, A.M. Keeler, Q. Su, L. Qui, S.A. Shaffer, Z. Xu, G. Gao, M. Sena-Esteves, Systemic AAV9 gene transfer in adult GM1 gangliosidosis mice reduces lysosomal storage in CNS and extends lifespan, Hum. Mol. Genet. 24 (2015) 4353–4364.
[15] C. Wyman, R. Kanaar, DNA double-strand break repair: all's well that ends well, Annu. Rev. Genet. 40 (2006) 363–383.
[16] L.S. Symington, J. Gautier, Double-strand break end resection and repair pathway choice, Annu. Rev. Genet. 45 (2011) 247–271.
[17] J.R. Chapman, M.R. Taylor, S.J. Boulton, Playing the end game: DNA double-strand break repair pathway choice, Mol. Cell 47 (2012) 497–510.
[18] P. Mali, L. Yang, K.M. Esvelt, J. Aach, M. Guell, J.E. Dicarlo, J.E. Norville, G.M. Church, RNA-Guided Human Genome Engineering via Cas9, Science 339 (2013) 823–826.
[19] Y. Fu, J.D. Sander, D. Reyon, V.M. Cascio, J.K. Joung, Improving CRISPR-Cas nuclease specificity using truncated guide RNAs, Nat. Biotechnol. 32 (2014) 279–284.
[20] T. Aida, K. Chiyo, T. Usami, H. Ishikubo, R. Imahashi, Y. Wada, K.F. Tanaka, T. Sakuma, T. Yamamoto, K. Tanaka, Cloning-free CRISPR/Cas system facilitates functional cassette knock-in in mice, Genome Biol. 16 (2015) 87.
[21] W. Wang, P.M. Kutny, S.L. Byers, C.J. Longstaff, M.J. Dacosta, C. Pang, Y. Zhang, R.A. Taft, F.W. Buaas, H. Wang, Delivery of Cas9 Protein into Mouse Zygotes through a Series of Electroporation Dramatically increases the Efficiency of Model creation, J. Genet. Genomics 43 (2016) 319–327.
[22] S.T. Yen, M. Zhang, J.M. Deng, S.J. Usman, C.N. Smith, J. Parker-Thornburg, P.G. Swinton, J.F. Martin, R.R. Behringer, Somatic mosaicism and allele complexity induced by CRISPR/Cas9 RNA injections in mouse zygotes, Dev. Biol. 393 (2014) 3–9.
[23] E.C. Hauser, J.L. Kasperzyk, A. D'Azzo, T.N. Seyfried, Inheritance of lysosomal acid β-galactosidase activity and gangliosides in crosses of DBA2J and knockout mice, Biochem. Genet. 42 (2004) 241–257.
[24] N. Kasai, L.O. Sillerud, R.K. Yu, A Convenient Method for the Preparation of Asialo-GM1, Lipids 17 (1982) 107–110.
[25] R.J. Carter, J. Morton, S.B. Dunnett, Motor Coordination and Balance in Rodents, Curr. Protocols Neurosci. (2001) 8.12.11–18.12.14.
[26] A.L. Southwell, J. Ko, P.H. Patterson, Intrabody gene therapy ameliorates motor, cognitive, and neuropathological symptoms in multiple mouse models of Huntington's disease, J. Neurosci. 29 (2009) 13589–13602.
[27] N. Ogawa, Y. Hirose, S. Ohara, T. Ono, Y. Watanabe, A simple quantitative bradykinesia test in MPTP-treated mice, Res. Commun. Chem. Pathol. Pharmacol. 50 (1985) 435–441.
[28] E. Hockly, B. Woodman, A. Mahal, C.M. Lewis, G. Bates, Standardization and statistical approaches to therapeutic trials in the R6/2 mouse, Brain Res. Bull. 61 (2003) 469–479.
[29] M. Jeyarkumar, T.D. Butters, M. Cortina-Borja, V. Hunnam, R.L. Proia, V.H. Perry, R.A. Dwek, F.M. Platt, Delayed symptom onset and increased life expectancy in Sandhoff disease mice treated with N-butyldeoxynojirimycin, Proc. Natl. Acad. Sci. U. S. A. 96 (1999) 6388–6393.
[30] C.A. Barnes, Memory Deficits Associated with Senescence: a Neurophysiological and Behavioral Study in the, Rat J. Comp. Physiol. Psychol. 93 (1979) 74–104.
[31] R. Gerlai, A new continuous alternation task in T-maze detects hippocampal dysfunction in mice. A strain comparison and lesion study, Behav. Brain Res. 95 (1998) 91–101.
[32] J.D. McCarter, D.L. Burgoyne, S. Miao, S. Zhang, J.W. Callahan, S.G. Wither, Identification of Glu-268 as the catalytic nucleophile of human lysosomal, J. Biol. Chem. 272 (1997) 396–400.
[33] M. Stemmer, T. Thumberger, M. Del Sol Keyer, J. Wittbrodt, J.L. Mateo, CCTop: an intuitive, flexible and reliable CRISPR/Cas9 target prediction tool, PLoS One 10 (2015) e0124633.
[34] A. Rosenberg, N. Stern, Changes in sphingosine and fatty acid components of the gangliosides in developing rat and human brain, J. Lipid Res. 7 (1966) 122–131.
[35] G. Müller, S. Alldinger, A. Moritz, A. Zurbriggen, N. Kirchhof, A. Sewell, W. Baumgärtner, GM1-gangliosidosis in Alaskan huskies: clinical and pathologic findings, Vet. Pathol. 38 (2001) 281–290.
[36] B.F. Porter, B.C. Lewis, J.F. Edwards, J. Alroy, B.J. Zeng, P.A. Torres, K.N. Bretzlaff, E.H. Kolodny, Pathology of GM2 gangliosidosis in Jacob sheep, Vet. Pathol. 48 (2011) 807–813.
[37] A. Berardelli, J.C. Rothwell, P.D. Thompson, M. Hallett, Pathophysiology of bradykinesia in Parksonson's disease, Brain 124 (2001) 2131–2146.
[38] L. Ou, T. Herzog, B.L. Koniar, R. Gunther, C.B. Whitley, High-dose enzyme replacement therapy in murine Hurler syndrome, Mol. Genet. Metab. 111 (2014) 116–122.
[39] L. Ou, M.J. Przybilla, B. Koniar, C.B. Whitley, RTB lectin-mediated delivery of lysosomal alpha-l-iduronidase mitigates disease manifestations systemically including the central nervous system, Mol. Genet. Metab. 123 (2018) 105–111.
[40] L. Ou, M.J. Przybilla, C.B. Whitley, SAAMP 2.0: an algorithm to predict genotype-phenotype correlation of lysosomal storage diseases, Clin. Genet. 93 (2018) 1008–1014.
[41] G. Venn, R.M. Mason, Absence of keratan sulphate from skeletal tissues of mouse and rat, Biochem. J. 228 (1985) 443–450.
[42] S. Chakravarti, T. Magnuson, J.H. Lass, K.J. Jepsen, C. Lamantia, H. Carroll, Lumican Regulates Collagen Fibril Assembly: Skin Fragility and Corneal Opacity in the Absence of Lumican, J. Cell Biol. 141 (1998) 1277–1286.
[43] S. Ying, A. Shiraishi, C.W.C. Kao, R.L. Converse, J.L. Funderburgh, J. Swiergiel, M.R. Rother, G.W. Conrad, W.W.Y. Kao, Characterization and expression of the mouse lumican gene, J. Biol. Chem. 272 (1997) 30306–30313.
[44] U. Ohto, K. Usui, T. Ochi, K. Yuki, Y. Satow, T. Shimizu, Crystal structure of human beta-galactosidase: structural basis of Gm1 gangliosidosis and morquio B diseases, J. Biol. Chem. 287 (2012) 1801–1812.
[45] T. Kobayashi, I. Goto, S. Okada, T. Orii, K. Ohno, T. Nakano, Accumulation of lysosphingolipids in tissues from patients with GM1 and GM2 gangliosidosis, J. Neurochem. 59 (1992) 1452–1458.
[46] K. Suzuki, K. Suzuki, S. Kamoshita, Chemical pathology of GM1-gangliosidosis (generalized gangliosidosis), J. Neuropathol. Exp. Neurol. 28 (1969) 25–73.
[47] D.A. Siegel, S.U. Walkley, Growth of ectopic dendrites on cortical pyramidal neurons in neuronal storage diseases correlates with abnormal accumulation of GM2 ganglioside, J. Neurochem. 62 (1994) 1852–1862.
[48] S. Grassi, E. Chiricozzi, L. Mauri, S. Sonnino, A. Prinetti, Sphingolipids and neuronal degeneration in lysosomal storage disorders, J. Neurochem. (2018), https://doi.org/10.1111/jnc.14540 (in press).
[49] J. Condori, W. Acosta, J. Ayala, V. Katta, A. Flory, R. Martin, J. Radin, C.L. Cramer, D.N. Radin, Enzyme replacement for GM1-gangliosidosis: Uptake, lysosomal activation, and cellular disease correction using a novel beta-galactosidase:RTB lectin fusion, Mol. Genet. Metab. 117 (2016) 199–209.
[50] M.L. Broekman, R.C. Baek, L.A. Comer, J.L. Fernandez, T.N. Seyfried, M. Sena-Esteves, Complete correction of enzymatic deficiency and neurochemistry in the GM1-gangliosidosis mouse brain by neonatal adeno-associated virus-mediated gene delivery, Mol. Ther. 15 (2007) 30–37.
[51] V.J. McCurdy, A.K. Johnson, H.L. Gray-Edwards, A.N. Randle, B.L. Brunson, N.E. Morrison, N. Salibi, J.A. Johnson, M. Hwang, R.J. Beyers, S.G. Leroy, S. Maitland, T.S. Denney, N.R. Cox, H.J. Baker, M. Sena-Esteves, D.R. Martin, Sustained Normalization of Neurological Disease after Intracranial Gene Therapy in a Feline Model, Sci. Transl. Med. 6 (2014).
[52] L. Ou, M.J. Przybilla, C.B. Whitley, Proteomic analysis of mucopolysaccharidosis I mouse brain with two-dimensional polyacrylamide gel electrophoresis, Mol. Genet. Metab. 120 (2017) 101–110.
[53] L. Ou, M.J. Przybilla, C.B. Whitley, Metabolomics profiling reveals profound metabolic impairments in mice and patients with Sandhoff disease, Mol. Genet. Metab. (2018), https://doi.org/10.1016/j.ymgme.2018.09.005 (in press).